

Discovery of magnetic A supergiants: the descendants of magnetic main sequence B stars[★]

Coralie Neiner^{1,†}, Mary E. Oksala^{2,1}, Cyril Georgy³, Norbert Przybilla⁴,
Stéphane Mathis^{5,1}, Gregg Wade⁶, Matthias Kondrak⁴, Luca Fossati⁷,
Aurore Blazère^{8,1}, Bram Buysschaert^{1,9}, and Jason Grunhut¹⁰,

¹LESIA, Observatoire de Paris, PSL Research University, CNRS, Sorbonne Universités, UPMC Univ. Paris 06, Univ. Paris Diderot, Sorbonne Paris Cité, 5 place Jules Janssen, 92195 Meudon, France

²Department of Physics, California Lutheran University, 60 West Olsen Road #3700, Thousand Oaks, CA 91360, USA

³Geneva Observatory, University of Geneva, chemin des Maillettes 51, 1290 Sauverny, Switzerland

⁴Institut für Astro- und Teilchenphysik, Universität Innsbruck, Technikerstr. 25/8, 6020, Innsbruck, Austria

⁵Laboratoire AIM Paris-Saclay, CEA/DRF - CNRS - Université Paris Diderot, IRFU/DAP Centre de Saclay, 91191 Gif-sur-Yvette, France

⁶Department of Physics, Royal Military College of Canada, PO Box 17000 Kingston, ON K7K 7B4, Canada

⁷Space Research Institute, Austrian Academy of Sciences, Schmiedlstrasse 6, A-8042, Graz, Austria

⁸Institut d’Astrophysique et de Géophysique, Université de Liège, Quartier Agora (B5c), Allée du 6 août 19c, 4000 Sart Tilman, Liège, Belgium

⁹Instituut voor Sterrenkunde, KU Leuven, Celestijnenlaan 200D, 3001 Leuven, Belgium

¹⁰Dunlap Institute for Astronomy and Astrophysics, University of Toronto, 50 St George Street, Toronto, ON M5S 3H4, Canada

Accepted XXX. Received YYY; in original form ZZZ

ABSTRACT

In the context of the high resolution, high signal-to-noise ratio, high sensitivity, spectropolarimetric survey BritePol, which complements observations by the BRITE constellation of nanosatellites for asteroseismology, we are looking for and measuring the magnetic field of all stars brighter than $V=4$. In this paper, we present circularly polarised spectra obtained with HarpsPol at ESO in La Silla (Chile) and ESPaDOnS at CFHT (Hawaii) for 3 hot evolved stars: ι Car, HR 3890, and ϵ CMa. We detected a magnetic field in all 3 stars. Each star has been observed several times to confirm the magnetic detections and check for variability. The stellar parameters of the 3 objects were determined and their evolutionary status was ascertained employing evolution models computed with the Geneva code. ϵ CMa was already known and is confirmed to be magnetic, but our modeling indicates that it is located near the end of the main sequence, i.e. it is still in a core hydrogen burning phase. ι Car and HR 3890 are the first discoveries of magnetic hot supergiants located well after the end of the main sequence on the HR diagram. These stars are probably the descendants of main sequence magnetic massive stars. Their current field strength (a few G) is compatible with magnetic flux conservation during stellar evolution. These results provide observational constraints for the development of future evolutionary models of hot stars including a fossil magnetic field.

Key words: stars: magnetic field – stars: early-type – stars: supergiants – stars: evolution – stars: individual: ι Car, HR 3890, ϵ CMa

1 INTRODUCTION

The evolution of OB stars on the Hertzsprung-Russell (HR) diagram depends on their initial mass, metallicity, rotation, and mass loss. The two latter parameters are affected by the

[★] Based on observations obtained at the Canada-France-Hawaii Telescope (CFHT) operated by the National Research Council of Canada, the Institut National des Sciences de l’Univers of the CNRS of France, and the University of Hawaii, and at the European Southern Observatory (ESO), Chile (program ID 094.D-0274A, 094.D-0274B, and 095.D-0155A).

[†] E-mail: coralie.neiner@obspm.fr

presence and evolution of a stellar magnetic field. Stellar evolution can also be influenced by the presence of a companion (Langer 2012). Because of the many parameters and effects at play in the evolution of OB stars, it remains difficult to establish clear evolutionary sequences among observed spectral types. Stellar evolution models, however, help to trace how these hot stars evolve. In particular, Groh et al. (2014) and Martins & Palacios (2017) showed that, for a star with an initial mass above $60 M_{\odot}$, the supergiant classification (luminosity class I) is already attributed to stars that are still on the main sequence (MS).

However, in current stellar evolution models, the role of the fossil magnetic field observed in $\sim 10\%$ of hot stars (Grunhut & Neiner 2015; Grunhut et al. 2017) is generally not taken into account. Attempts have been made to include a Taylor-Spruit dynamo field in stellar evolution codes (e.g. Maeder & Meynet 2003; Heger et al. 2005), however it has been shown that such dynamos likely do not exist in MS hot stars (Zahn et al. 2007; Neiner et al. 2015). The effect of a stable dipolar field has also been recently investigated in stellar models, but mainly as a surface effect impacting the wind (Petit et al. 2017; Georgy et al. 2017) or for its impact on a given structure (Duez et al. 2010).

The fossil fields of hot MS stars are expected to be highly influential in the context of stellar structure and evolution (e.g. Moss 1984; Maeder & Meynet 2014). The basic consequences of magnetic fields for stellar evolution fall into two general categories: (i) interaction of interior fields with interior fluid motions, impacting the internal rotational profile, angular momentum, and chemical transport (e.g. Mestel 1999; Mathis & Zahn 2005; Sundqvist et al. 2013); and (ii) interaction of surface fields with the stellar wind, leading to magnetic braking of surface layers and reduction of the surface mass-loss rate (ud-Doula & Owocki 2002; ud-Doula et al. 2008, 2009; Meynet et al. 2011). For example, studies of magnetic Herbig Ae/Be have shown that their magnetic field brakes their rotation rate during the early phases of their lives (Alecian et al. 2013a), and evidence for spindown on the MS has also been found in hotter stars (e.g. Townsend et al. 2010). Recent studies also suggest, and in some cases demand, that magnetic fields have direct and ubiquitous consequences for evolution. For example, in order to explain the post-MS gap of blue supergiants, Petermann et al. (2015) have proposed that these objects evolve from magnetic MS stars. In addition, Maeder & Meynet (2014) have examined the role of strong, organized fields in the cores of red supergiants, with implications for the general spin rates of (magnetic) white dwarfs and pulsars. Ultimately, these effects lead to important modification of stellar evolutionary pathways and stellar feedback effects, such as mechanical energy deposition in the interstellar medium and supernova explosions (Heger et al. 2005), and hence the properties of stellar remnants and potentially the structure and chemistry of the local Galactic environment.

As magnetic fields influence stellar evolution, so are magnetic fields expected to transform in response to changes in the structure of the stars in which they are embedded. In particular, as hot stars age, their radius expands dramatically. The evolution of surface magnetic fields of hot stars during the MS has been investigated by Bagnulo et al. (2006), Landstreet et al. (2007, 2008), and Fossati et al. (2016). These studies provide convincing evidence that the

strengths of surface magnetic fields decrease systematically during the MS, in response to stellar expansion (the stellar radius typically expands by a factor of ~ 3 between the zero age MS and the terminal age MS), and possibly due to Ohmic decay and other (currently unknown) mechanisms. Because hot giants and supergiants retain the radiative envelopes they had on the MS, evolved OBA stars provide a capability to directly extend the existing studies of MS objects (such as MiMeS, Grunhut et al. 2017) to more advanced evolutionary phases and a much greater range of stellar structural changes. Considering that about 10% of all hot stars host a fossil magnetic field on the MS (Grunhut & Neiner 2015; Fossati et al. 2015b; Grunhut et al. 2017), it is expected that a similar fraction of hot supergiants could also show magnetic fields of fossil origin at their surface.

In addition, as hot stars age more and more, convective regions appear in their radiative envelope. Local dynamos probably develop in these convective zones, providing an opportunity to also study the unique interactions between the post-MS dynamo and the pre-existing fossil field. In particular, it is expected that the dynamo-fossil interaction could enhance the local dynamo fields and modify the configuration of the global fossil field (Featherstone et al. 2009a; Aurière et al. 2008). Extensive surveys of magnetic fields in cool (F, G, K) giants and supergiants (the even older evolutionary descendants of OBA MS stars) have already shown that many of these cool stars exhibit magnetic fields powered by dynamos (e.g. Grunhut et al. 2010; Aurière et al. 2015). Although a small population of red giants still show evidence of fossil fields surviving from the MS (e.g. Aurière et al. 2008), the growth of a fully convective envelope, which replaces the radiative envelope, appears to effectively erase evidence of their earlier magnetic characteristics at the surface, even though the fossil field probably still exists inside the star.

Understanding the evolution of the fossil magnetic fields observed in hot MS stars is thus important to understand the evolution of these stars. Finding and understanding magnetic hot supergiants is therefore crucial. However, only two claimed OB supergiants have been found to host a magnetic field so far. The O9.5 supergiant ζ Ori Aa hosts a dipolar magnetic field of ~ 140 G at the pole (Bouret et al. 2008; Blazère et al. 2015). However, its radius is only $\sim 20 R_{\odot}$ (Hummel et al. 2013); therefore it appears to be a very young supergiant. According to the Bonn stellar evolution models, this star is indeed only at about the middle of its MS lifetime (see Fig. 2 of Fossati et al. 2015a). In the same way, the B1.5 star ϵ CMa was found to be magnetic with a polar field strength of at least 13 G, but its evolutionary status is unclear: either it is still in its MS phase or already a post-MS object (Fossati et al. 2015a). Attempts to detect magnetic fields in other hot supergiants led to no detection (e.g. Grunhut et al. 2010; Shultz et al. 2014), likely due to the insufficient precision of the spectropolarimetric measurements compared to the expected field strength. As of today, there are thus no clearly evolved magnetic hot stars known.

In this paper, we present new observations of ϵ CMa and of two other hot supergiant stars: ι Car and HR 3890 (Sect. 2). We report the determination of their stellar parameters and evolutionary status (Sect. 3), and the detection of their magnetic field (Sect. 4). We then discuss the link between magnetic hot supergiants and MS magnetic massive

stars in the framework of the fossil and dynamo field scenarios (Sect. 5).

2 OBSERVATIONS

2.1 BritePol, the BRITE spectropolarimetric survey

The BRITE (BRiGht Target Explorer) constellation of nanosatellites focuses on the monitoring of stars with $V \leq 4$, with high-precision, high-cadence photometry, in order to perform asteroseismology and to study stellar variability due to stellar and planetary companions, tidal interactions, and rotation (Weiss et al. 2014). The BRITE sample consists of apparently bright stars, therefore it is dominated by hot stars at all evolutionary stages and evolved cooler stars (cool giants and AGB stars), which are the most intrinsically luminous stars.

In this framework, we are performing a spectropolarimetric survey of all targets with $V \leq 4$, i.e. about 600 stars, with the goal of discovering new bright magnetic stars and thus providing prime targets for BRITE seismic studies. Discovering new bright magnetic stars is also important to provide targets for multi-technique studies, e.g. including both spectropolarimetric and interferometric observations.

Spectropolarimetric observations of each of the ~ 600 targets ($V \leq 4$), that are not yet available from archives, have been gathered with three high-resolution spectropolarimeters: Narval at the Télescope Bernard Lyot (TBL) in France, ESPaDOnS at the Canada-France-Hawaii Telescope (CFHT) in Hawaii, and HarpsPol on the ESO 3.6-m telescope in La Silla.

In this paper, we report the detection of magnetic fields in 3 hot supergiant stars obtained with HarpsPol and ESPaDOnS.

2.2 Spectropolarimetric observations

The spectropolarimetric observations presented here have been acquired with ESPaDOnS at CFHT (Hawaii) and HarpsPol at the ESO 3.6-m telescope (La Silla, Chile). The log of observations is available in Table 1.

ESPaDOnS covers a wavelength range from about 375 to 1050 nm, with a resolving power of ~ 68000 , spread over 40 echelle orders projected onto a single detector. HarpsPol covers a shorter wavelength range from about 380 to 690 nm on two detectors and 71 echelle orders, but with a higher resolving power of ~ 110000 .

We observed the targets in circular polarisation mode. Each observation consists of four sub-exposures taken with the polarimeter in various configurations. The four sub-exposures are constructively combined to obtain the Stokes V spectrum and destructively combined to produce a null polarisation profile (N) to check for pollution by, e.g., instrumental effects, variable observing conditions, or physical phenomena unrelated to magnetism such as pulsations. In addition, the intensity (Stokes I) spectrum is extracted. Finally, successive sequences can be acquired and co-added to increase the signal-to-noise ratio (S/N) of a magnetic measurement.

The usual calibrations (bias, flat-field, and ThAr

Table 1. Journal of observations indicating the name of the stars, the instrument used for the spectropolarimetric measurements (H=HarpsPol, E=ESPaDOnS), the Heliocentric Julian Date at the middle of the observations (mid-HJD - 2450000), the exposure time in seconds, and the average signal-to-noise ratio of a spectropolarimetric sequence per CCD pixel at ~ 500 nm.

Star	Inst.	Date	mid-HJD -2450000	T_{exp}	S/N
ι Car	H	Nov 9, 2014	6970.8666	4×34	420
ι Car	H	Nov 10, 2014	6971.8472	5×4×55	510
ι Car	H	Mar 2, 2015	7083.6199	4×55	500
ι Car	H	Mar 3, 2015	7084.5692	3×4×75	560
ι Car	H	Mar 9, 2015	7090.6508	3×4×75	700
HR 3890	H	Mar 9, 2015	7090.6638	4×119	650
HR 3890	H	May 13, 2015	7155.5660	4×125	725
ϵ CMa	E	Feb 8, 2014	6696.8619	4×7	775
ϵ CMa	E	Nov 9, 2014	6971.1382	9×4×7	1270
ϵ CMa	E	Dec 22, 2014	7014.0850	9×4×7	1080
ϵ CMa	E	Jan 9, 2015	7032.0893	9×4×7	1010

frames) have been obtained each night and applied to the data. The ESPaDOnS data reduction was performed using LIBRE-ESPRIT (Donati et al. 1999) and UPENA, a dedicated software pipeline available at CFHT. The Stokes I spectra were normalized to the continuum level, order by order, using IRAF¹, and the same normalization function was applied to the Stokes V and N spectra. The HarpsPol reduction was performed with a modified version of the REDUCE package (Piskunov & Valenti 2002; Makaganiuk et al. 2011). Automatic normalization was first performed with REDUCE and an additional normalization function was fitted with IRAF to improve the final normalization.

Finally, we applied the Least Squares Deconvolution (LSD) technique (Donati et al. 1997) to produce the mean LSD Stokes I, Stokes V, and N profiles of each magnetic measurement. Consecutive sequences of observations of the same star were then co-added to produce one single magnetic measurement.

LSD requires a list of all lines present in the spectrum, including their wavelength, depth, and Landé factor. Such a line mask was produced for each of the three targets. We first extracted lists of lines from the VALD3 atomic database (Piskunov et al. 1995; Kupka et al. 1999) for the appropriate temperature and gravity of each star (determined in Sect. 3 below, also see Table 2). We restricted the lists to lines with a depth larger than 0.01. We then removed from each mask all lines that are not present in the observed intensity spectra, hydrogen lines because their profile is different from those of metal lines, and lines blended with either H lines, interstellar lines, or telluric lines. In addition, in the case of the mask for the hottest star ϵ CMa, we removed the He lines with broad wings (see Fossati et al. 2015a, and Wade et al. in prep.). Finally, the depth of each line in the LSD masks was adjusted so as to fit the observed line depth. This method is described in more details in Grunhut et al. (2017).

¹ IRAF is distributed by the National Optical Astronomy Observatory, which is operated by the Association of Universities for Research in Astronomy (AURA) under a cooperative agreement with the National Science Foundation.

Table 2. Parameters for the three stars ι Car, HR 3890, and ϵ CMa. Columns report the star name, spectral type, effective temperature, gravity, luminosity, mass at the ZAMS, rotation rate at the ZAMS, radius at the ZAMS, current mass, current radius, and age. For each star, the results from the two most extreme evolutionary models reproducing simultaneously T_{eff} , $\log(g)$, and $\log(L/L_{\odot})$ are shown, to illustrate the range of possible initial conditions.

Star	SpT	T_{eff} K	$\log(g)$ cm s $^{-2}$	$\log(L/L_{\odot})$	M_{ZAMS} M_{\odot}	$\frac{\Omega_{\text{ZAMS}}}{\Omega_{\text{crit}}}$	R_{ZAMS} R_{\odot}	M M_{\odot}	R R_{\odot}	age Myr
ι Car	A7Ib ¹	7500 ± 100	1.85 ± 0.10	4.53 ± 0.37^2	7.0	0.30	3.00	6.90	46.4-50.1	56.35-56.40
					11.0	0.10	3.82	10.96	69.1-72.7	18.88
HR 3890	A7Ib	7500 ± 100	1.4 ± 0.1	–	11.0	0.9	4.32	10.88	96.6-100.0	23.42-23.44
					15.0	0.00	4.48	14.70	134.6-141.3	11.52-11.53
ϵ CMa	B1.5II	22500 ± 300^3	3.4 ± 0.08^3	4.35 ± 0.05^3	12.0	0.30	4.00	11.92	10.4-10.5	17.62-17.88
					12.0	0.80	4.31	11.91	10.4	18.86-18.96

Notes: taken from ¹Gray & Garrison (1989), ²Boyarchuk & Lyubimkov (1984), and ³Fossati et al. (2015a).

3 STELLAR PARAMETERS

3.1 Determination of the atmospheric parameters

The star ι Car was classified as A7Ib by Gray & Garrison (1989). HR 3890 is the supergiant primary of a visual binary, with the 3.2 mag fainter B3-4IV secondary (HR 3891, Mandrini & Niemela 1986) located only 5'' away. The companion, however, is sufficiently far away not to be recorded in the HarpsPol spectra presented here, since Harps's fibers have a diameter of 1''. The spectra of ι Car and HR 3890 are almost identical, except for some metal lines and the Balmer wings that indicate a slightly higher luminosity for HR 3890. The H α profile is symmetric and in absorption. We therefore assign a spectral type of A7Ib to HR 3890 as well, similar to the earlier A8Ib classification by Houk & Cowley (1975). ϵ CMa is one of the two primary standards defining the B1.5II class in the MK system (Gray & Corbally 2009). Both the spectral types and the luminosity classification provide guidance for the starting points of the quantitative analysis.

The determination of the atmospheric parameters of ι Car and HR 3890 is based on the hybrid non-LTE (local thermodynamic equilibrium) approach described by Przybilla et al. (2006) and Farnstein & Przybilla (2012) for the analysis of BA-type supergiants. In brief, the modelling is based on plane-parallel, hydrostatic, chemically homogeneous and line-blanketed model atmospheres that were computed with the code ATLAS9 (Kurucz 1993) under the assumption of LTE. Sphericity may be considered an issue for the extended atmospheres of supergiants. However, these two stars are near the lower luminosity boundary of the supergiant class. The atmospheres have an extension of only 1–2% of the stellar radius, therefore deviations from plane-parallel geometry can be considered negligible. The onset of convection in stellar atmospheres occurs among the mid/late A-type stars. We therefore considered convective energy transport using the standard Böhm-Vitense mixing-length theory (Böhm-Vitense 1958) employed in the ATLAS9 code, adopting a ratio of mixing length to pressure scale height of 1.5. The fraction of the total energy flux transported by convection remains below 1% in both cases.

In a second step, non-LTE level populations and synthetic spectra were calculated with recent versions of the codes DETAIL and SURFACE (Giddings 1981; Butler & Giddings 1985). Here, essential extensions to the work of Przybilla et al. (2006) consist of i) the implementation of ad-

ditional bound-free and free-free opacities appropriate for cooler temperatures (most important H $^{-}$, plus metals with low first ionisation threshold), ii) consideration of collisions with neutral hydrogen atoms (using the formula of Steenbock & Holweger 1984), iii) inclusion of self-broadening for the Balmer lines (Barklem et al. 2000b), and iv) Van-der-Waals broadening using coefficients from Barklem et al. (2000a), the collection of Kurucz² or approximations (see, e.g., Castelli 2005).

We focused on simultaneous fits to the Stark-broadened hydrogen Balmer lines and the Mg I/II ionization equilibrium in order to constrain the effective temperature T_{eff} and surface gravity $\log g$. Model atoms as described by Przybilla et al. (2001) and Przybilla & Butler (2004) were employed for the two species, with the above mentioned modifications. The derived atmospheric parameter values are summarized in Table 2. Our T_{eff} value for ι Car is in good agreement with previous determinations by Luck & Lambert (1985, 1992), Smiljanic et al. (2006) and Tanriverdi & Baştürk (2016), while our surface gravity value is higher than in most of these works ($\log g = 0.9$ to 1.6), and significantly lower than the $\log g = 2.3$ derived by Smiljanic et al. (2006). In the case of HR 3890, atmospheric parameters have so far been reported only by Samedov (1988), $T_{\text{eff}} = 7600 \pm 350$ K and $\log g = 1.1 \pm 0.3$, which agree with our results within the uncertainties.

The atmospheric parameter determination for ϵ CMa was described in detail by Fossati et al. (2015a) and these parameters are reported in Table 2. The same model codes as employed here for the A-type supergiants were used for ϵ CMa by Fossati et al. (2015a), following the analysis strategy and adopting model atoms as summarized by Nieva & Przybilla (2012).

3.2 Evolutionary status

Determining the evolutionary status and stellar parameters, such as the initial mass, current age, etc., for post-MS phases of massive stars on the basis of stellar evolution models is not a straightforward task, and is extremely dependent on the stellar evolution code used to build the models, due to various ways of implementing physical processes (convection, rotation, overshooting,...) inside such codes.

² <http://kurucz.harvard.edu/linelists.html>

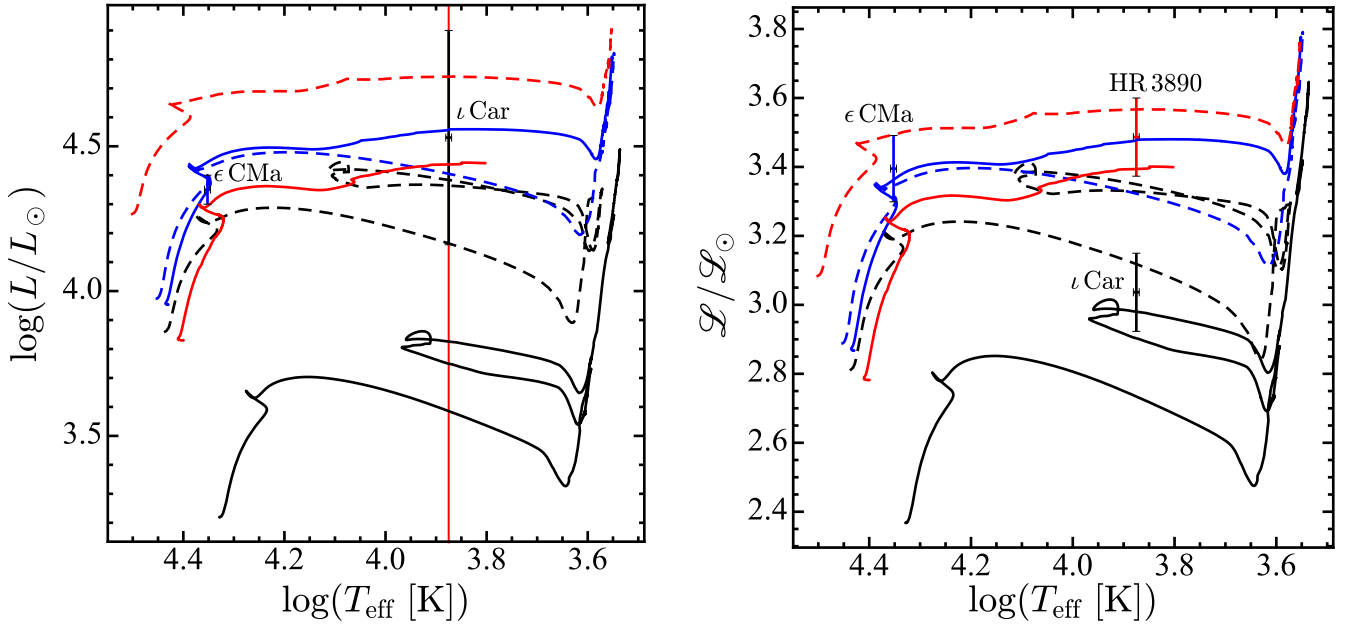


Figure 1. *Left panel:* HR diagram of our models compared to the observed position of ι Car and ϵ CMa. The black tracks correspond to the two most extreme models fitting the position of ι Car: $7 M_{\odot}$ with $\Omega_{\text{ZAMS}}/\Omega_{\text{crit}} = 0.30$ (solid) and $11 M_{\odot}$ with $\Omega_{\text{ZAMS}}/\Omega_{\text{crit}} = 0.10$ (dashed). The blue tracks correspond to the two most extreme models fitting the position of ϵ CMa: $12 M_{\odot}$ with $\Omega_{\text{ZAMS}}/\Omega_{\text{crit}} = 0.8$ (solid) and $12 M_{\odot}$ with $\Omega_{\text{ZAMS}}/\Omega_{\text{crit}} = 0.3$ (dashed). The red tracks correspond to the two most extreme models fitting the position of HR 3890: $11 M_{\odot}$ with $\Omega_{\text{ZAMS}}/\Omega_{\text{crit}} = 0.9$ (solid) and non-rotating $15 M_{\odot}$ (dashed). As we have found no measurement of the luminosity of HR 3890 in the literature, we only show its effective temperature with the thin vertical red line. Note, however, that the spectrum of HR 3890 indicates a slightly higher luminosity than for ι Car. *Right panel:* tracks of our models in the spectroscopic HR diagram (Langer & Kudritzki 2014),

where $\mathcal{L} = T_{\text{eff}}^4/g$. The observational errors on \mathcal{L} are computed as $\Delta\mathcal{L} = \sqrt{\left(\frac{4AT_{\text{eff}}}{T_{\text{eff}}}\right)^2 + \Delta\log(g)^2}$. The colors and line styles are the same as in the left panel.

In this paper, we used different sets of models computed with the Geneva stellar evolution code (Eggenberger et al. 2008) at solar metallicity and including the effects of rotation (Ekström et al. 2012; Georgy et al. 2013). To refine our determination of the evolutionary status, we have also computed several additional models, using exactly the same code and physical ingredients³. We stress that none of the models presented in this paper include a magnetic field, since evolutionary models computed including the physical influence of a fossil field in the radiative envelope of hot stars do not exist yet (see Sect. 1).

For each star, we fit simultaneously the available observational data. The effective temperature and surface gravity were determined from our spectra (see Sect. 3.1). We also accounted for the luminosity when this quantity was available from the literature, i.e. for ι Car and ϵ CMa.

The results for each individual star are discussed below. The last six columns of Table 2 give the initial mass, the initial rotation rate, the initial radius, the current mass, the current radius, and the permitted age range. For each star, the results of the two most extreme models (smaller and higher initial mass) are shown. In Fig. 1, we show how the tracks compare to the observations in the classical (left) and spectroscopic (right) HR diagram.

³ These models, however, were computed only up to the base of the red supergiant branch, which is enough for the purpose of this paper.

3.2.1 ι Car

ι Car has an effective temperature $T_{\text{eff}} = 7500 \pm 100$ K and a surface gravity of $\log(g) = 1.85 \pm 0.10$ from our determinations. From this determination, the constraint on the models are quite weak (right panel of Fig. 1): from $\sim 7 M_{\odot}$ (solid black curve) up to $\sim 11 M_{\odot}$ (dashed black curve). Adding a constraint on the luminosity ($\log(L) = 4.53 \pm 0.37$, Boyarchuk & Lyubimkov 1984) allows us to tighten the estimate (left panel), limiting the mass to about $11 M_{\odot}$. We remark that the luminosity estimate from Boyarchuk & Lyubimkov (1984) was based on a different set of stellar models and does not come from direct independent measurements.

In all cases, ι Car is clearly a post-MS star. Depending on its mass, it could be on its first crossing of the HR diagram (if its mass is closer to $11 M_{\odot}$), or on a blue loop (if its mass is closer to $7 M_{\odot}$). Its age is between ~ 19 and 56 Myr, depending on its mass. Other quantities such as the current mass and radius can be found in Table 2. On the MS, ι Car was a B star.

3.2.2 HR 3890

In the case of HR 3890, no distance is available to determine its luminosity. Therefore, we rely on our estimates of T_{eff} and $\log(g)$ only. For these two quantities, we have obtained $T_{\text{eff}} = 7500 \pm 100$ K and $\log(g) = 1.4 \pm 0.1$, which provide good constraints (right panel of Fig. 1). The star is also clearly a post-MS star. According to the set of models we

Table 3. Results of the magnetic field measurements for the 3 stars ι Car, HR 3890 and ϵ CMa. The first four columns provide the name of the star, the longitudinal field (B_l) and null (N_l) measurements in Gauss, with their error bars, and detection status (DD = definite detection, ND = no detection), for each magnetic measurement. The last two columns indicate the inferred magnetic polar field strength in Gauss, as it currently is (B_p) assuming a dipole field and as it was on the MS (B_{MS}) assuming magnetic flux conservation, for each star.

Star	$B_l \pm \sigma B_l$	$N_l \pm \sigma N_l$	Detect.	B_p	B_{MS}
ι Car	-0.8 ± 0.5	-0.3 ± 0.5	ND	3	700-1100
ι Car	-0.9 ± 0.2	-0.1 ± 0.2	DD		
ι Car	-0.4 ± 0.4	0.1 ± 0.4	ND		
ι Car	-0.5 ± 0.2	0.1 ± 0.2	ND		
ι Car	-0.3 ± 0.2	-0.1 ± 0.2	ND		
HR 3890	-1.9 ± 1.1	-0.6 ± 1.1	ND	6	3000-6000
HR 3890	-1.0 ± 1.0	-1.1 ± 1.0	ND		
ϵ CMa	-1.2 ± 10.9	-4.5 ± 10.9	DD	32	185-220
ϵ CMa	-9.1 ± 2.1	1.6 ± 2.1	DD		
ϵ CMa	-9.6 ± 2.5	1.6 ± 2.5	DD		
ϵ CMa	-6.3 ± 2.9	0.2 ± 2.9	DD		

used, its mass is higher than the maximal mass for which a Cepheid blue loop occurs. This star is therefore on its first (and unique) crossing of the HR diagram. The range of possible models goes from a rotating $11 M_\odot$ star with an initial angular velocity of 90% of the critical velocity to a non-rotating $15 M_\odot$ star. The age would be between ~ 11.5 Myr up to ~ 23.5 Myr, depending on the initial mass. The current radius of the star ranges from ~ 96 to $\sim 141 R_\odot$. On the MS, HR 3890 was a B star.

3.2.3 ϵ CMa

For ϵ CMa, we used the stellar parameters from Fossati et al. (2015a). They obtained $T_{\text{eff}} = 22500 \pm 300$ K, $\log(g) = 3.40 \pm 0.08$, and $\log(L/L_\odot) = 4.35 \pm 0.05$. From our evolutionary models, we obtain that the initial mass of the star should be very close to $12 M_\odot$, with an initial angular velocity in the range of 30% to 80% of the critical velocity. The only solution simultaneously fitting the effective temperature, the luminosity and the surface gravity is a model near the end of the MS (see both panels of Fig. 1). The age of the star is between ~ 17.5 and ~ 19 Myr, and the current radius is around $10.5 R_\odot$.

4 MAGNETIC ANALYSIS AND RESULTS

For each spectropolarimetric measurement, using a center-of-gravity method (Rees & Semel 1979; Wade et al. 2000), we calculate the longitudinal field value B_l corresponding to the Zeeman signatures observed in the LSD Stokes V profiles. We do the same for the N profiles.

In addition, the detection of a magnetic field is evaluated by the False Alarm Probability (FAP) of a signature in the LSD Stokes V profile inside the velocity range defined by the LSD I line width, compared to the mean noise level in the LSD Stokes V profile outside the line. We adopted the convention defined by Donati et al. (1997): if $\text{FAP} < 0.001\%$, the magnetic detection is definite, if $0.001\% < \text{FAP}$

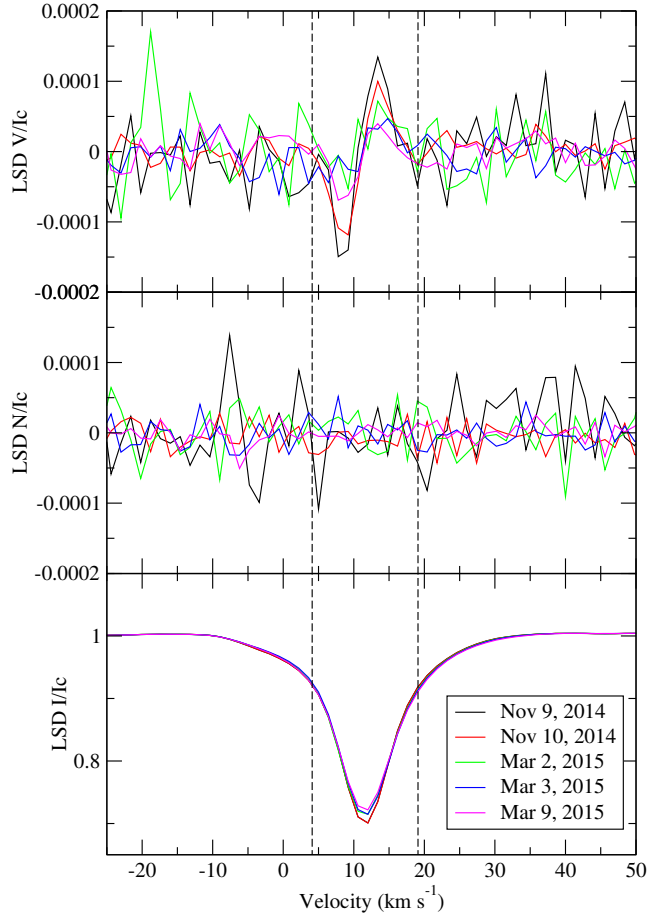


Figure 2. LSD Stokes V (top), N (middle) and Stokes I (bottom) profiles for the star ι Car, taken on 5 different nights. Vertical dashed lines indicate the integration range employed to calculate the longitudinal field and estimate the FAP.

$< 0.1\%$ the detection is marginal, otherwise there is formally no magnetic detection.

Results for the three stars are shown in Table 3 and described below.

4.1 ι Car

ι Car has been observed five times with HarpsPol in November 2014 and March 2015. Each measurement consisted of one or more consecutive Stokes V sequences of 4 subexposures of 34 to 75 seconds each, i.e. a total exposure time between 136 and 1100 seconds per magnetic measurement (see Table 1). The line mask produced for this star includes 7014 lines. The LSD profiles have a S/N ranging from 2360 to 5300 in Stokes I, and 15000 to 44000 in Stokes V.

While the magnetic signature is clearly visible in all 5 measurements of ι Car (see Fig. 2), only the second measurement, taken close to the pole-on phase and with a very high S/N, results formally in a definite detection. For the other measurements, the signature is too weak compared to the noise level in the continuum. Nevertheless, the observed signature, present at the position of the intensity line profile and which varies in time in the way expected from a dipole field, leaves no doubt that ι Car is magnetic. The magnetic

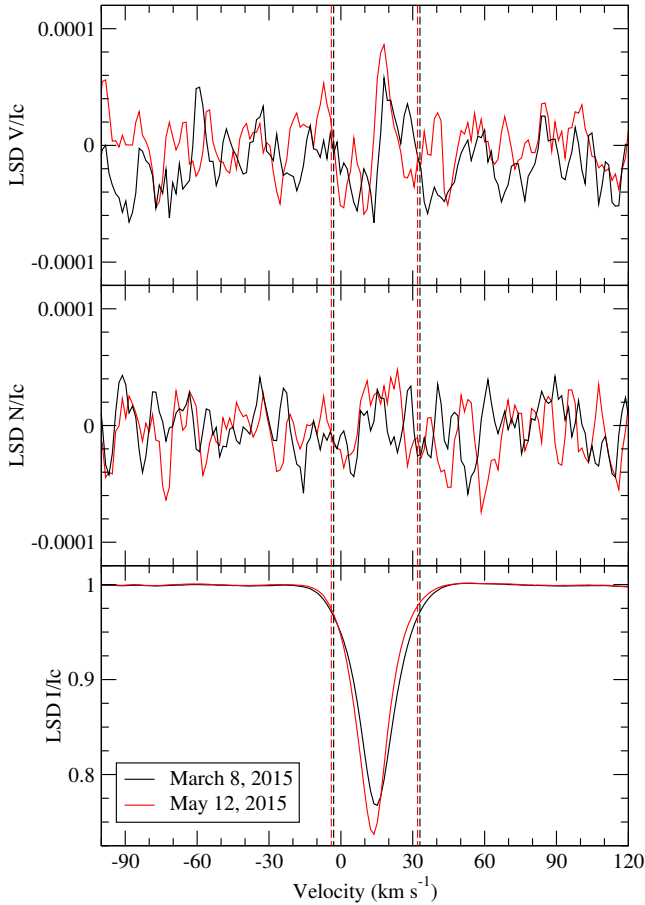


Figure 3. Same as Fig. 2, but for the two measurements of the star HR 3890.

signature, however, is only visible in the core of the LSD line. Broad wings are often observed in the spectral lines of hot supergiants and could be due to strong macroturbulence (see Simón-Díaz et al. 2017). We also note that small variations are visible in the core of the intensity profile.

From these Stokes V signatures and the corresponding I profiles, we calculated the longitudinal field values by integrating in a range of $\pm 7.5 \text{ km s}^{-1}$ around the center of the line (at 11.6 km s^{-1}), thus excluding the broad wings. B_l values are reported in Table 3. The longitudinal field is systematically negative at the rotational phases at which the data were acquired and below 1 G in strength. Similar measurements performed with the N profiles provide values compatible with 0 (see Table 3).

In addition, from the weak variation observed in the Stokes V signatures and in the B_l values for data acquired during a few nights in each of the two periods of observation and 4 months apart between the two periods, we conclude that the rotation period of ι Car is probably long, of at least a few months. Follow-up observations of this target should allow an accurate determination of the star’s rotation period.

4.2 HR 3890

HR 3890 has been observed twice with HarpsPol, once in March 2015 and once in May 2015. Each measurement con-

sisted of a single Stokes V sequence of 4 subexposures of either 119 or 125 seconds each, respectively, i.e. a total exposure time of 476 and 500 seconds per magnetic measurement (see Table 1). The line mask produced for this star includes 5448 lines. The LSD profiles have a respective S/N of 3060 and 3040 in Stokes I, and 18316 and 20598 in Stokes V.

A weak but clear signature is visible in the Stokes V profile of both measurements, with a similar shape in spite of the ~ 2 months difference in observation date and variation in the intensity profile (see Fig. 3).

Following the example of ι Car, we excluded the line wings from the calculation of the longitudinal field values. We thus integrated the two Stokes V signatures and the corresponding I profiles in a range of $\pm 18 \text{ km s}^{-1}$ around the center of the line (15 and 14 km s^{-1} , respectively for the two measurements). B_l values are reported in Table 3. The field is systematically negative and between -1 and -2 G in strength. Similar measurements (N_l) were also performed with the N profiles. Although the second B_l value is compatible with 0 within the error bars and no formal detection is obtained from the FAP analysis for any of the two measurements (see Table 3), the fact that Stokes V profiles show a clear and repeatable signature, while N profiles show only noise, provides confidence that the magnetic signature is real.

4.3 ϵ CMa

ϵ CMa has been observed four times with ESPaDOnS in February, November, December 2014, and January 2015. The first measurement consisted of only one single Stokes V sequence of 4 subexposures of 7 seconds each, i.e. a total exposure time of 28 seconds. The following 3 measurements consisted of 9 consecutive Stokes V sequences of 4 subexposures of 7 seconds each, i.e. a total exposure time of 252 seconds per magnetic measurement (see Table 1). The line mask produced for this star includes 1746 lines. The LSD profiles have a S/N from 3989 to 4803 in Stokes I and 23405 to 119309 in Stokes V.

All four LSD profiles provide a definite detection according to the FAP analysis, with clear magnetic signatures in Stokes V and no signal in N. We integrated the four Stokes V signatures and the corresponding I profiles in a range of $27.5 \pm 42.5 \text{ km s}^{-1}$, i.e. again excluding the broad wings. B_l values are reported in Table 3. For the first (shorter) measurement, the longitudinal field has a relatively large error bar, but the next 3 (longer) measurements all show longitudinal fields of the order of -6 to -10 G. Similar measurements (N_l) were also performed with the N profiles and are compatible with 0.

5 DISCUSSION

5.1 Magnetic detections

We confirm that the B star ϵ CMa is magnetic, as discovered by Fossati et al. (2015a). However, we find that it is located at the end of the MS and it is not yet a post-MS object, as already suspected by Fossati et al. (2015a). It is nevertheless classified as a bright giant (B1.5II) in the literature, likely due to its He II line. This is frequently the case for massive stars in the second part of the MS, as shown by Martins &

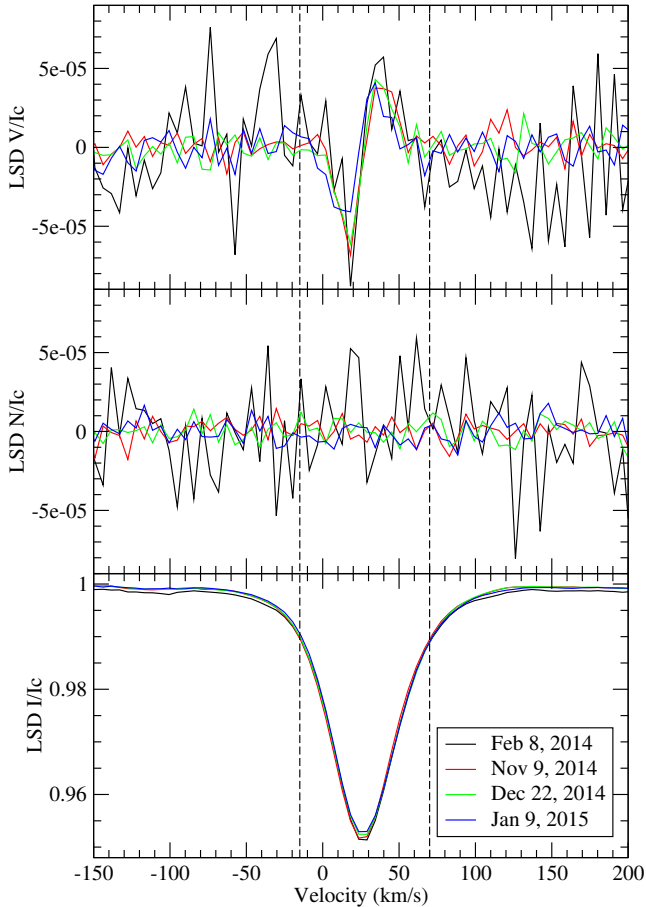


Figure 4. Same as Fig. 2, but for the four measurements of the star ϵ CMa.

Palacios (2017). In the same way, the O star ζ Ori Aa was confirmed to be magnetic by Blazère et al. (2015), but its small radius ($\sim 20 R_{\odot}$, Hummel et al. 2013) and its position on evolutionary tracks (Fossati et al. 2015a) suggest that it is a very young supergiant still on the MS. Until now, there were thus no known clearly evolved (post-MS) magnetic hot supergiants.

In this work, we find that ι Car and HR 3890 are two magnetic A7Ib supergiants. Evolutionary models presented in this work leave no doubt about their strongly evolved supergiant status, well beyond the MS, and the magnetic signatures in the stars are clear.

We recall that the evolutionary models used in this work do not include a magnetic field. It is known that a magnetic field can modify the evolution of the star. In particular, it can brake the stellar rotation, reduce its effective mass loss, and also modify its internal structure and rotation profile. Without a magnetic stellar evolution code, it is not possible to provide quantitative estimates of how the magnetic field did and will modify the evolution of the stars we have studied here. Our results, however, provide observational constraints to future evolutionary models with fossil magnetic fields that are currently under development.

Since our determination of the current evolutionary status of the targets studied here is based on their spectra and not on the models, the current evolutionary status presented

above is certain. However, the stellar parameters derived for the stars at the ZAMS could be over- or under-estimated because of the lack of magnetic fields in the evolutionary models.

5.2 Origin of the magnetic field in hot supergiants

Following the two detections of magnetic fields in supergiant stars presented in this work, the possible origin of these fields must be discussed. With this aim, we computed Kippenhahn diagrams for both stars (see Fig. 5) from the evolutionary models presented above. They provide the evolution (without a magnetic field) of the stellar internal structure as a function of time relative to the last computed time step (t_f). The respective radial extension of convective and stably stratified radiative regions are represented in gray and white, respectively, while the red line indicates the stellar surface. In the case of ι Car, the star is currently in a transition phase: a convective external region is developing above its large radiative envelope and a small convective core. In the case of HR 3890, the star has already passed this transition phase but only a very thin convective layer has developed in the radiative envelope.

Since the external layers of both stars are currently still mostly radiative, and have remained mainly radiative during the entire post-MS evolution so far, the most plausible hypothesis is that the current magnetic field is the same field as those observed in B-type stars on the MS, i.e. a fossil field (Braithwaite & Nordlund 2006; Duez & Mathis 2010), which has been conserved. To verify this hypothesis, we can use magnetic flux conservation to infer the strength of the fossil field the stars would have hosted during their MS stage, using the stars' current and MS radius estimates. We obtain a MS field between ~ 700 G and ~ 1100 G for ι Car and between ~ 3 and ~ 6 kG for HR 3890, respectively (see Table 3, which also indicates a MS field for ϵ CMa of about 200 G). These values correspond to the typical fossil field strength observed in magnetic Bp or Ap stars on the MS (e.g. Grunhut & Neiner 2015), therefore magnetic flux conservation appears to be plausible. This does not imply that magnetic flux conservation alone has occurred, but simply that it is a sufficient explanation. If these magnetic supergiants started their lives with a stronger magnetic field, magnetic decay could also have occurred, as observed on the MS (Bagnulo et al. 2006; Landstreet et al. 2007, 2008; Fossati et al. 2016). In addition, the radius on the MS may be slightly larger/smaller when including a magnetic field in the evolutionary models (Duez et al. 2010), hence the MS field might be slightly different as well.

In spite of the agreement between the derived MS field for our targets and typical fossil field strengths observed in magnetic Bp or Ap stars on the MS, we investigated the possible role of the central convective core of each star. First, they have a very small radius (of the order of $0.1 R_{\odot}$) when compared to the total radius of the star (of the order of $100 R_{\odot}$). Therefore, even if a dynamo action is at work in the core (Brun et al. 2005), the field generated in these layers would have a large distance to cross to reach the surface of the star. In this framework, MacGregor & Cassinelli (2003) demonstrated that the time needed for a flux tube generated in the core of a massive MS star to emerge at the stellar surface is longer than the lifetime of the star. This time is

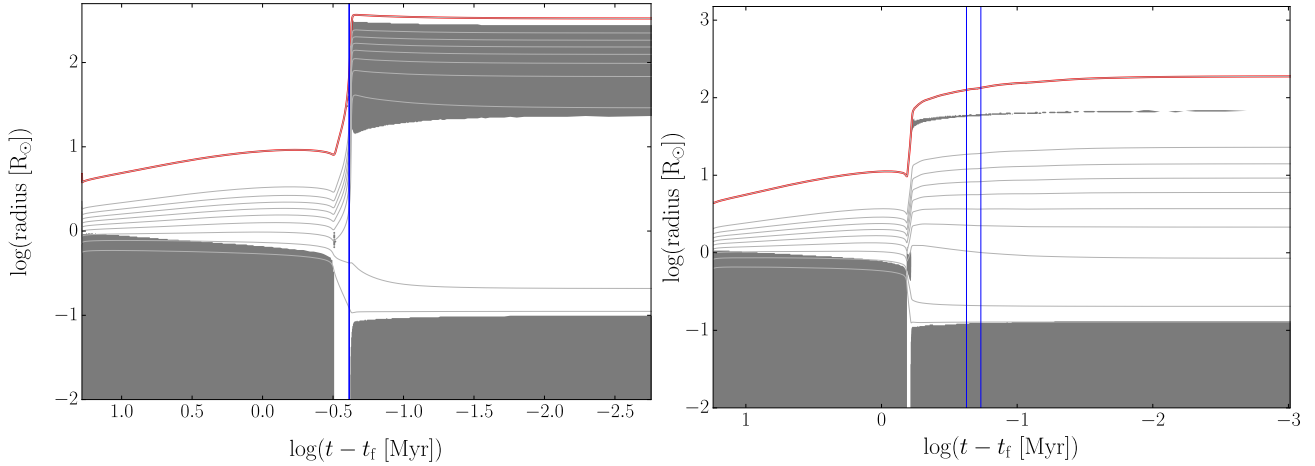


Figure 5. Kippenhahn diagrams showing the evolution of the stellar structure of ι Car (left) and HR 3890 (right). Convective zones are indicated in gray, while radiative zones are in white. The red line indicates the surface of the star and the thin gray lines show the mass distribution for 11 regular steps between 0 and the initial mass value of the star. The vertical blue lines show the current position of the star in this diagram, within uncertainties.

even longer in a supergiant star. Therefore, we conclude that it is not possible that the fields observed at the surface are those generated in the convective core.

A dynamo could also develop in the intermediate thin convective layer of HR 3890. The same argument as for the convective core however applies: the layer is very thin and located too deep (in the middle of the radiative envelope) for a potential dynamo field to reach the surface. According to our models, ι Car did not reach the phase where a large external convective zone develops yet, and its Zeeman signature looks simple, as expected from a dipolar field, rather than complex, as expected from a dynamo field in a convective shell.

Finally, the impact of the intermediate thin convective layer of HR 3890 on its fossil field is examined. Because of the small radial extent of this convective layer relatively to the global size of the star, we may infer that it has not significantly perturbed the fossil field configuration in the external radiative envelope during the star’s evolution. Indeed, a similar situation occurs earlier in the life of the star, when it transitions from the pre-MS Herbig phase to the MS. During this transition, the appearance of a convective core does not affect the fossil field in the radiative region (Alecian et al. 2013b). However, it is possible that the obliquity of the fossil field changes, because of its coupling with the dynamo fields likely present in the core and in the intermediate convective shell (Featherstone et al. 2009b).

From the above discussion, we conclude that the magnetic fields observed at the surface of ι Car and HR 3890 are probably the remnants of the fields present on the MS, i.e. they are fossil fields.

6 CONCLUSIONS

In this paper we confirm that ϵ Cma is magnetic, as discovered by Fossati et al. (2015a), but we find that it is near the end of the MS rather than a post-MS star. In addition, we present the detections of two new magnetic A7 supergiant stars, which are more evolved: ι Car and HR 3890. Their cur-

rent weak field is compatible with the strength of fossil fields observed on the MS if we consider magnetic flux conservation as the principal agent driving evolution of their surface magnetic field strengths. Moreover, the shape and slow evolution with time of their Zeeman signatures also point towards fossil fields. Therefore, these magnetic A supergiants are the probable descendants of magnetic MS B stars. Monitoring of their field variability over a full rotation period with further spectropolarimetric observations will allow us to verify the fossil origin of these fields and model their geometry and strength.

In the future it will also be interesting to find magnetic hot supergiants that are even more evolved and with a large external convective region that has developed on top of the radiative envelope (i.e. a hotter, more evolved version of ι Car). Their fossil fields should be even weaker than those presented here, and those fields could possibly be more complex if they are mixed with dynamo effects developing in the convective surface envelope (Augustson et al. 2017). Their observation will thus require ultra-deep spectropolarimetric observations.

Finally, the results presented here provide observational constraints for the current development of evolutionary models of hot stars including a fossil magnetic field.

ACKNOWLEDGEMENTS

CN and AB acknowledge support from the ANR (Agence Nationale de la Recherche) project Imagine. CN, MO, SM, AB, and BB acknowledge support from PNPS (Programme National de Physique Stellaire). MK acknowledges support by the Austrian Science Fund FWF within the DK-ALM (W1259-N27). Part of the research leading to these results has received funding from the European Research Council (ERC) under the European Union’s Horizon 2020 research and innovation programme (grant agreements number 670519: MAMSIE and 647383: SPIRE). GAW acknowledges Discovery Grant support from the Natural Sciences and Engineering Research Council (NSERC) of Canada.

This research has made use of the SIMBAD database operated at CDS, Strasbourg (France), and of NASA's Astrophysics Data System (ADS).

REFERENCES

- Alecian E., Wade G. A., Catala C., Grunhut J. H., Landstreet J. D., Böhm T., Folsom C. P., Marsden S., 2013a, *MNRAS*, **429**, 1027
- Alecian E., Neiner C., Mathis S., Catala C., Kochukhov O., Landstreet J., 2013b, *A&A*, **549**, L8
- Augustson K., Mathis S., Brun A. S., Toomre J., 2017, preprint, ([arXiv:1702.04227](https://arxiv.org/abs/1702.04227))
- Aurière M., et al., 2008, *A&A*, **491**, 499
- Aurière M., et al., 2015, *A&A*, **574**, A90
- Bagnulo S., Landstreet J. D., Mason E., Andretta V., Silaj J., Wade G. A., 2006, *A&A*, **450**, 777
- Barklem P. S., Piskunov N., O'Mara B. J., 2000a, *A&AS*, **142**, 467
- Barklem P. S., Piskunov N., O'Mara B. J., 2000b, *A&A*, **363**, 1091
- Blazère A., Neiner C., Tkachenko A., Bouret J.-C., Rivinius T., 2015, *A&A*, **582**, A110
- Böhm-Vitense E., 1958, *Z. Astrophys.*, **46**, 108
- Bouret J.-C., Donati J.-F., Martins F., Escolano C., Marcolino W., Lanz T., Howarth I. D., 2008, *MNRAS*, **389**, 75
- Boyarchuk A. A., Lyubimov L. S., 1984, *Astrophysics*, **20**, 57
- Braithwaite J., Nordlund Å., 2006, *A&A*, **450**, 1077
- Brun A. S., Browning M. K., Toomre J., 2005, *ApJ*, **629**, 461
- Butler K., Giddings J. R., 1985, in *Newsletter of Analysis of Astronomical Spectra*, No. 9 (Univ. London)
- Castelli F., 2005, *Memorie della Societa Astronomica Italiana Supplementi*, **8**, 44
- Donati J.-F., Semel M., Carter B. D., Rees D. E., Collier Cameron A., 1997, *MNRAS*, **291**, 658
- Donati J.-F., Catala C., Wade G. A., Gallou G., Delaigüe G., Rabou P., 1999, *A&AS*, **134**, 149
- Duez V., Mathis S., 2010, *A&A*, **517**, A58
- Duez V., Mathis S., Turck-Chièze S., 2010, *MNRAS*, **402**, 271
- Eggenberger P., Meynet G., Maeder A., Hirschi R., Charbonnel C., Talon S., Ekström S., 2008, *Ap&SS*, **316**, 43
- Ekström S., et al., 2012, *A&A*, **537**, A146
- Featherstone N. A., Browning M. K., Brun A. S., Toomre J., 2009a, *ApJ*, **705**, 1000
- Featherstone N. A., Browning M. K., Brun A. S., Toomre J., 2009b, *ApJ*, **705**, 1000
- Firnstein M., Przybilla N., 2012, *A&A*, **543**, A80
- Fossati L., et al., 2015a, *A&A*, **574**, A20
- Fossati L., et al., 2015b, *A&A*, **582**, A45
- Fossati L., et al., 2016, *A&A*, **592**, A84
- Georgy C., Ekström S., Granada A., Meynet G., Mowlavi N., Eggenberger P., Maeder A., 2013, *A&A*, **553**, A24
- Georgy C., Meynet G., Ekström S., Wade G. A., Petit V., Keszthelyi Z., Hirschi R., 2017, *A&A*, **599**, L5
- Giddings J. R., 1981, PhD thesis, Univ. London
- Gray R. O., Corbally J. C., 2009, *Stellar Spectral Classification*
- Gray R. O., Garrison R. F., 1989, *ApJS*, **70**, 623
- Groh J. H., Meynet G., Ekström S., Georgy C., 2014, *A&A*, **564**, A30
- Grunhut J. H., Neiner C., 2015, in Nagendra K. N., Bagnulo S., Centeno R., Jesús Martínez González M., eds, *IAU Symposium Vol. 305, Polarimetry*. pp 53–60
- Grunhut J. H., Wade G. A., Hanes D. A., Alecian E., 2010, *MNRAS*, **408**, 2290
- Grunhut J. H., et al., 2017, *MNRAS*, **465**, 2432
- Heger A., Woosley S. E., Spruit H. C., 2005, *ApJ*, **626**, 350
- Houk N., Cowley A. P., 1975, *University of Michigan Catalogue of two-dimensional spectral types for the HD stars. Volume I. Declinations –90 to –53°*.
- Hummel C. A., Rivinius T., Nieva M.-F., Stahl O., van Belle G., Zavala R. T., 2013, *A&A*, **554**, A52
- Kupka F., Piskunov N., Ryabchikova T. A., Stempels H. C., Weiss W. W., 1999, *A&AS*, **138**, 119
- Kurucz R., 1993, *ATLAS9 Stellar Atmosphere Programs and 2 km/s grid*. Kurucz CD-ROM No. 13. Cambridge, Mass.: Smithsonian Astrophysical Observatory, 1993., **13**
- Landstreet J. D., Bagnulo S., Andretta V., Fossati L., Mason E., Silaj J., Wade G. A., 2007, *A&A*, **470**, 685
- Landstreet J. D., et al., 2008, *A&A*, **481**, 465
- Langer N., 2012, *ARA&A*, **50**, 107
- Langer N., Kudritzki R. P., 2014, *A&A*, **564**, A52
- Luck R. E., Lambert D. L., 1985, *ApJ*, **298**, 782
- Luck R. E., Lambert D. L., 1992, *ApJS*, **79**, 303
- MacGregor K. B., Cassinelli J. P., 2003, *ApJ*, **586**, 480
- Maeder A., Meynet G., 2003, *A&A*, **411**, 543
- Maeder A., Meynet G., 2014, *ApJ*, **793**, 123
- Makaganiuk V., et al., 2011, *A&A*, **525**, A97
- Mandrini C. H., Niemela V. S., 1986, *MNRAS*, **223**, 79
- Martins F., Palacios A., 2017, *A&A*, **598**, A56
- Mathis S., Zahn J.-P., 2005, *A&A*, **440**, 653
- Mestel L., 1999, *Stellar magnetism*
- Meynet G., Eggenberger P., Maeder A., 2011, *A&A*, **525**, L11
- Moss D., 1984, *MNRAS*, **209**, 607
- Neiner C., Mathis S., Alecian E., Emeriau C., Grunhut J., BinaM-IcS MiMeS Collaborations 2015, in Nagendra K. N., Bagnulo S., Centeno R., Jesús Martínez González M., eds, *IAU Symposium Vol. 305, Polarimetry*. pp 61–66
- Nieva M.-F., Przybilla N., 2012, *A&A*, **539**, A143
- Petermann I., Langer N., Castro N., Fossati L., 2015, *A&A*, **584**, A54
- Petit V., et al., 2017, *MNRAS*, **466**, 1052
- Piskunov N. E., Valenti J. A., 2002, *A&A*, **385**, 1095
- Piskunov N. E., Kupka F., Ryabchikova T. A., Weiss W. W., Jeffery C. S., 1995, *A&AS*, **112**, 525
- Przybilla N., Butler K., 2004, *ApJ*, **609**, 1181
- Przybilla N., Butler K., Becker S. R., Kudritzki R. P., 2001, *A&A*, **369**, 1009
- Przybilla N., Butler K., Becker S. R., Kudritzki R. P., 2006, *A&A*, **445**, 1099
- Rees D. E., Semel M. D., 1979, *A&A*, **74**, 1
- Samedov Z. A., 1988, *Izvestiya Ordena Trudovogo Znamenii Krymskoj Astrofizicheskoj Observatorii*, **79**, 57
- Shultz M., Wade G. A., Petit V., Grunhut J., Neiner C., Hanes D., MiMeS Collaboration 2014, *MNRAS*, **438**, 1114
- Simón-Díaz S., Godart M., Castro N., Herrero A., Aerts C., Puls J., Telting J., Grassitelli L., 2017, *A&A*, **597**, A22
- Smiljanic R., Barbuy B., de Medeiros J. R., Maeder A., 2006, *A&A*, **449**, 655
- Steenbock W., Holweger H., 1984, *A&A*, **130**, 319
- Sundqvist J. O., Petit V., Owocki S. P., Wade G. A., Puls J., MiMeS Collaboration 2013, *MNRAS*, **433**, 2497
- Tanriverdi T., Baştürk Ö., 2016, *New Astron.*, **47**, 46
- Townsend R. H. D., Oksala M. E., Cohen D. H., Owocki S. P., ud-Doula A., 2010, *ApJ*, **714**, L318
- Wade G. A., Donati J.-F., Landstreet J. D., Shorlin S. L. S., 2000, *MNRAS*, **313**, 851
- Weiss W. W., et al., 2014, *PASP*, **126**, 573
- Zahn J.-P., Brun A. S., Mathis S., 2007, *A&A*, **474**, 145
- ud-Doula A., Owocki S. P., 2002, *ApJ*, **576**, 413
- ud-Doula A., Owocki S. P., Townsend R. H. D., 2008, *MNRAS*, **385**, 97
- ud-Doula A., Owocki S. P., Townsend R. H. D., 2009, *MNRAS*, **392**, 1022

This paper has been typeset from a $\text{\TeX}/\text{\LaTeX}$ file prepared by the author.